Computer-Aided Design of *E*-Plane Waveguide Passive Components

PONG FAN AND DESEN FAN

Abstract—**The newly developed numerical analysis method for the inductive discontinuities in rectangular waveguide is presented. It can be used to analyze the scattering properties of *E*-plane uniform conductor–dielectric inserts in rectangular waveguide. These inserts are of arbitrary cross section and number. The calculation accuracy and speed are remarkably improved by a combined analytical–numerical approach. Some practical applications are given demonstrating its engineering usefulness.**

I. Introduction

MILLIMETER-WAVE technology has seen rapid progress recently. CAA and CAD techniques are in great demand due to the short wavelength and small waveguide size of millimeter waves. The basic question of waveguide passive components is one of analyzing the scattering properties of waveguide discontinuities. Schwinger and Marcuvitz provided excellent summaries of earlier work [1], [2]. But many theoretical approaches had not been brought into full play. Great progress has been achieved with the application of computer numerical techniques [3]–[7]. However all these methods are largely restricted to inserts of specific geometry, such as single circular posts or zero-thickness diaphragms [1]–[4], and less attention has been paid to the study of conductor–dielectric inserts, despite their theoretical and practical significance. Two excellent papers [5], [6] were published recently. For improving the infinite series convergence, Auda, on the basis of an integral equation of the conductor-induced currents, divided the Green's function into the static Green's function and its correction terms [5]. The counterpart dielectric case has been treated in a similar way by Hsu [6], based on an integral equation of the dielectric-polarized currents. The numerical results, as shown in [5] and [6], are satisfactory. However the available design data in [6] are only for circular lossless dielectric posts. This is not sufficient for practical millimeter engineering, due to the difficulty encountered in making high-dielectric-constant material into accurate circular posts of small size.

Our research interest is in exploring new numerical techniques and their corresponding universal algorithms. In this paper, based on the combined integral equation of the conductor-induced and dielectric-polarized currents, the scattering properties of inductive conductor–dielectric inserts in rectangular waveguide are analyzed by the moment method. The calculation accuracy and speed are remarkably improved by segmenting the integration region into dielectric rectangular or conductor line cells and applying analytic integration, cell by cell. The method is also applicable to arbitrary cross section inserts by properly selecting the number of cells. In Section IV, further practical examples are given, demonstrating that the method presented holds promise for microwave and millimeter-wave engineering.

Manuscript received January 4, 1988; revised July 12, 1988.

The authors are with the Department of Electronics, University of Science and Technology of China, Hefei, Auhui, China.

IEEE Log Number 8824982.

II. Theory

The configuration being investigated is shown in Fig. 1(a). It is assumed that $a < \lambda < 2a$ and that the incident wave is the dominant H_{10} mode traveling in the z direction. Since the inserts are uniform along the y axis and the incident field E_y^{in} has only a y component, which does not vary with y, the scattered modes are H_{m0}. So all the vector fields can be written in terms of scalar fields along the y axis. The scattered field is then given by

$$\begin{cases} E_{yc}^s = \int_{c_L} I_S(x_S, z_S) G(\tilde{r}_S, \tilde{r})\, dl \\ E_{yd}^s = -jKc\mu \int_{c_S} J_S(x_S, z_S) G(\tilde{r}_S, \tilde{r})\, dS \end{cases} \tag{1}$$

where c_L is the line integral along the conductor boundary, c_S is the surface integral in the dielectric region, I_S and J_S are the conductor-induced current density and dielectric-polarized current density, respectively, and

$$J_S(\tilde{r}) = -j\omega(\epsilon - \epsilon_0)E(x,z) = -jKc\epsilon_0(\epsilon_r - 1)E(x,z). \tag{2}$$

The subscripts c and d denote the conductor and the dielectric region, respectively. $G(\tilde{r}_S, \tilde{r})$ is Green's function denoting $G(x_S, z_S; x, z)$:

$$G(\tilde{r}_S, \tilde{r}) = \sum_{m=1}^{\infty} \frac{A}{\Gamma_m} \sin\left(\frac{m\pi}{a}x\right) \sin\left(\frac{m\pi}{a}x_S\right) e^{-\Gamma_m |z - z_S|} \tag{3}$$

where the constant $A = -j120\pi K/a$, $K = \omega\sqrt{\mu_0\epsilon_0}$ is the propagation constant, and $\Gamma_m = \sqrt{\left(\frac{m\pi}{a}\right)^2 - K^2}$. Based on

0018-9480/89/0200-0335$01.00 ©1989 IEEE

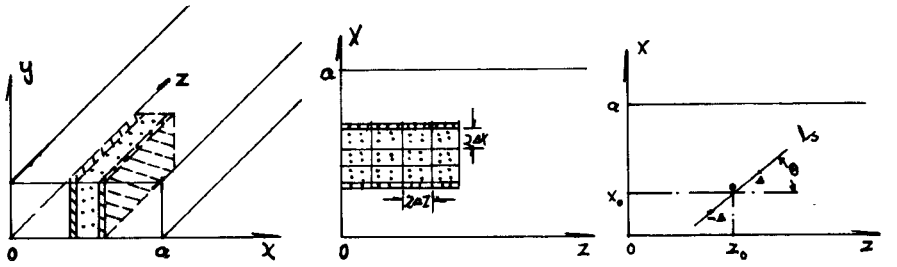

(a) (b) (c)

Fig. 1.

the field continuity,

$$\sin\left(\frac{\pi}{a}x\right)e^{-\Gamma_1 z} + E^s_{yc} = 0$$

$$\sin\left(\frac{\pi}{a}x\right)e^{-\Gamma_1 z} + E^s_{yd} = E^{\text{in}}_y. \tag{4}$$

Then we obtain the combined integral equation as follows:

$$-\sin\left(\frac{\pi}{a}x\right)e^{-\Gamma_1 z} = \int_{c_L} I_S(\tilde{r}_S)G(\tilde{r}_S,\tilde{r})\,dl$$

$$-jKc\epsilon_0(\epsilon_r+1)\sin\left(\frac{\pi}{a}x\right)e^{-\Gamma_1 z} = J_S(\tilde{r})$$

$$+K^2c^2\epsilon_0(\epsilon_r-1)\cdot\int_{c_S} J_S(\tilde{r}_S)G(\tilde{r}_S,\tilde{r})\,ds. \tag{5}$$

We divided the integration region into L equal rectangular cells Δs and N equal line cells Δl. I_S and J_S can be expressed as

$$J_S(\tilde{r}) = \sum_{K=1}^{L} J_K P_K(\tilde{r})$$

$$I_S(\tilde{r}) = \sum_{K=1}^{N} I_K P_K(\tilde{r}) \tag{6}$$

where the basis functions $P_K(\tilde{r})$ are defined as

$$P_K(\tilde{r}) = \begin{cases} 1 & \text{when } \tilde{r} \text{ in } \Delta s \text{ or } \Delta l \\ 0 & \text{elsewhere.} \end{cases} \tag{7}$$

The weighting function is defined as

$$W = \delta(\tilde{r}-\tilde{r}_q), \qquad q = 1,\cdots,L,L+1,\cdots,L+N. \tag{8}$$

We can generate a set of linear equations by first substituting (6) into (5) and then obtaining a scalar product on the resulting equation with the weighting function:

$$\sum_{K=L+1}^{L+N} I_K C^q_K = B^q, \qquad q = L+1,\cdots,L+N$$

$$\sum_{K=1}^{L} J_K A^q_K = B^q, \qquad q = 1,2,\cdots,L \tag{9}$$

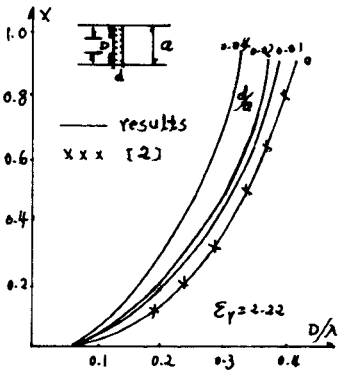

Fig. 2.

where

$$B^q = -E^{\text{in}}_y(\tilde{r}_q) = -\sin\left(\frac{\pi}{a}x_q\right)e^{-\Gamma_1 z_q}$$

$$A^q_K = jKc\int_{c_S} G(\tilde{r}_q,\tilde{r})\,ds + \frac{\delta^q_K}{jKc\epsilon_0(\epsilon_r-1)}$$

$$C^q_K = \int_{c_L} G(\tilde{r}_q,\tilde{r})\,dl$$

$$\delta^q_K = \begin{cases} 1, & q = K \\ 0, & q \neq K. \end{cases} \tag{10}$$

As can be seen in (9) and (10), solving the problem by the conventional moment method is extremely difficult. Because the matrix elements A^q_K and C^q_K involve an infinite series, which converges slowly, especially when $K = q$ as is the case for the cells themselves, the series is not convergent and the integral equation is singular. Therefore, obtaining useful results by simply truncating finite series is either unlikely or uneconomical. We find a combined analytical–numerical approach by applying segmental integration, thereby not only avoiding numerical integration but also improving the convergence remarkably. The segmental integration procedure is straightforward but tedious. Only the final expressions are presented (see the Appendix). From (A1)–(A4) of the Appendix, we notice that the convergence rate of the new infinite series is near $1/m^3$ when m is large, in contrast to the former, which is near $1/m$.

With (9) and (A1)–(A4), we can obtain the distribution of I_S and J_S. The scattering field can be obtained by substituting I_S and J_S into (1). Now we consider two

reference planes Z_{T1} and Z_{T2}:

$$Z_{T1} \leqslant \min(z_i, i=1,2,\cdots,L+N)$$
$$Z_{T2} \geqslant \max(z_i, i=1,2,\cdots,L+N). \quad (12)$$

Then the scattering coefficients can be represented as [4]

$$S_{11} = \frac{E_y^s|_{z_{T1}}}{E_y^{\text{in}}|_{z_{T1}}}$$
$$S_{21} = \frac{\left(E_y^{\text{in}} + E_y^s\right)|_{z_{T2}}}{E_y^{\text{in}}|_{z_{T2}}} \quad (13)$$

and the equivalent circuit parameters can be obtained [7].

III. Numerical Results

To check the program we consider a few selected cases for which data are available. Devices are also discussed in Section IV.

Fig. (2) shows the calculation reactance of the thin inductive diaphragm with and without a dielectric substrate. In practical applications, there are difficulties worth noting when the metal strip is either too thin or too thick. In the second case, it is difficult to guarantee the tolerance due to long etching time. A new treatment involves replacing the metal strips with copper-covered dielectric plate. In the latter case the structure is quite compatible with printed circuit technology. The method presented here can be applied in such a case naturally.

As to circular dielectric posts, shown in Fig. 3, based on the concept of "equivalent cross section," we approximate the polygonal cross section to the circular cross section by properly selecting the number of small cells. Fig. 4 shows the insertion loss as a function of frequency for a lossy rectangular dielectric post. We further analyze the conductor–dielectric insert cases, which have found many applications in engineering. The calculation results are also satisfactory, as shown in Fig. 5.

IV. E-Plane Filter Design

In this section, a few applications of our method are presented.

A. E-Plane Metal Bandpass Filter

Millimeter-wave applications of the conventional E-plane filter shown in Fig. 6(a) have attracted considerable attention over the past few years [8]–[10] for its low cost and mass producibility. But the performance deterioration in the second stopband presents a significant problem. To alleviate this, three different solutions have been proposed:

1) Increase the thickness of the metal inserts [10].
2) Use several layers of metal inserts rather than a single one [8].
3) Reduce the waveguide width in the vicinity of the strips [9].

However, we notice that though the response characteristics are improved, as expected, the complexity of structures partially offsets the advantage of the new configuration. The main feature of our solution is the use of conventional waveguide, combining transverse strips with longitudinal inserts, as shown in Fig. 6(c), and iris-coupled structures, as shown in Fig. 7(c), thereby not only keeping the simplicity of structure, but also obtaining good stopband attenuation properties. The design data of the filter have not been optimized; rather they were chosen on the basis of experience.

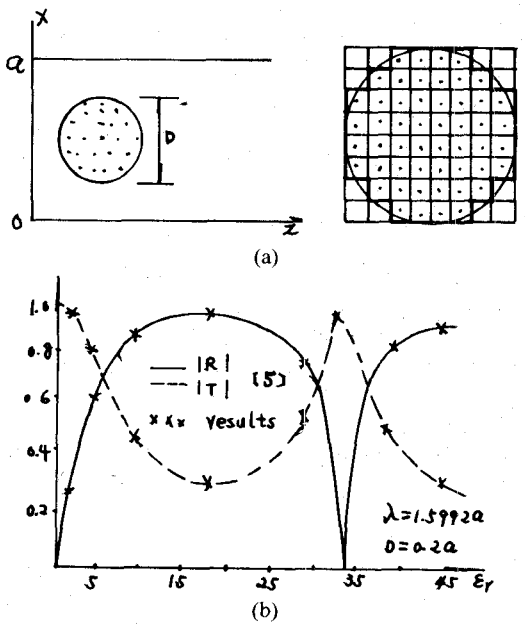

Fig. 3.

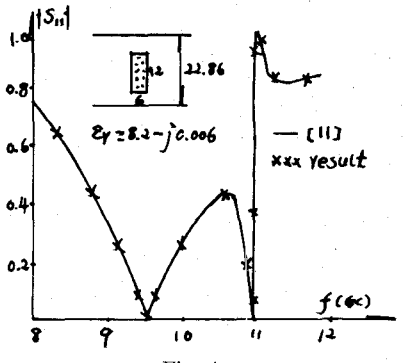

Fig. 4.

B. Wide-Band E-Plane Bandpass Filter

Fig. 8(a) shows the configuration of a wide-band E-plane bandpass filter, which consists of several resonators. The filter design is a symmetrical structure with the outermost strips the narrowest. With other design parameters fixed, these strips become narrower as the design bandwidth increases. So in practice, especially in the millimeter-wave band, it is rather difficult to attain the small size of edge strips. The range of validity for the E-plane filter design is limited by the dimensional tolerance that is required for reliable and reproducible design. We are enabled to achieve similar filter behavior by replacing edge strips with equivalent transverse strips, as shown in Fig. 8(b).

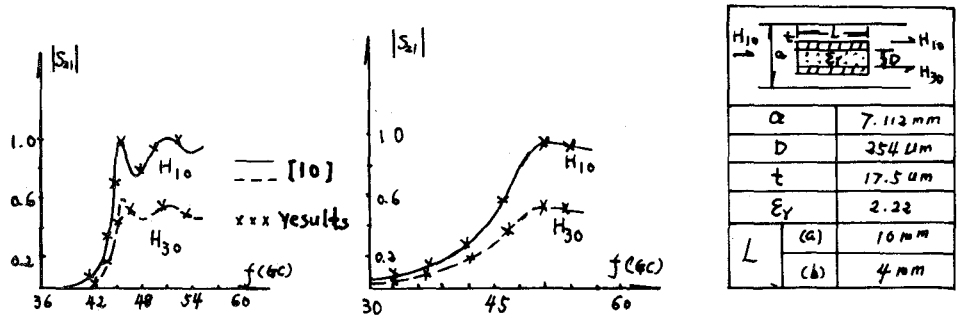

Fig. 5.

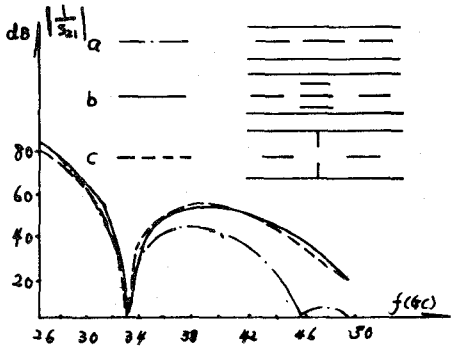

Fig. 6.

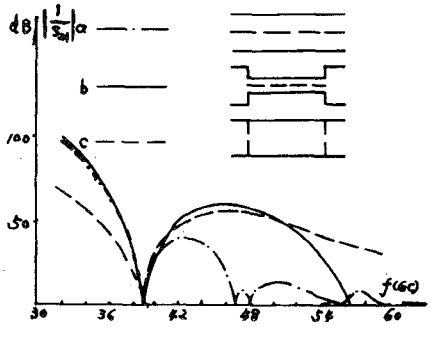

Fig. 7.

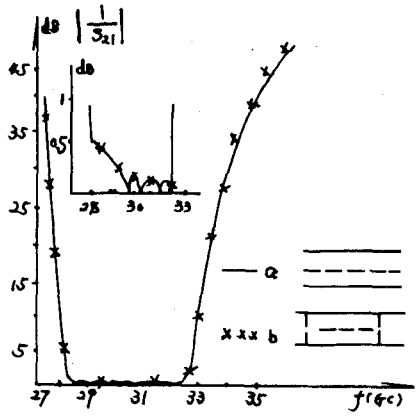

Fig. 8.

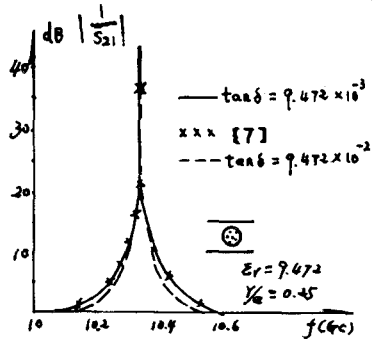

Fig. 9.

C. Dielectric Bandstop Filter

The design of a filter can be carried out at the points where the value of the dielectric constant and the size of the dielectric post make the coefficient R or T equal to zero. So dielectric bandpass and bandstop filters can be realized by the configurations of Fig. 3 and Fig. 4. Compared to conventional waveguide bandstop filters, the advantage of the dielectric bandstop filter is obvious. Fig. 9 shows the insertion loss as a function of frequency for a lossy circular dielectric post. Numerical results agree well with data in the literature. As to differing dielectric loss, we have the same resonant frequency, but the insertion loss curve will be smoother when $\tan\delta$ becomes larger.

V. Conclusion

A complete field analysis of all kinds of inductive discontinuities has been presented. Some practical examples are given, demonstrating its usefulness in practice. The entire work was carried out using IBM-PC/XT microcomputer.

Appendix

In this Appendix, the self-contributions and interactions of cells are presented. Corresponding signs are referred to Fig. 1(b) and Fig. 1(c)

1) Self-contribution of dielectric rectangular cell:

$$\Delta E_y(\tilde{r}) = \sum_{m=1}^{\infty} J_S(\tilde{r}_S)\frac{4Ba}{m\pi\Gamma_m^2}\sin^2\left(\frac{m\pi}{a}x\right)$$

$$\cdot\sin\left(\frac{m\pi}{a}\Delta x\right)\left(1-e^{-\Gamma_m\Delta z}\right). \quad \text{(A1)}$$

2) The contribution of the dielectric rectangular cell to other field point:

$$\Delta E_y(\tilde{r}) = \sum_{m=1}^{\infty} J_S(\tilde{r}_s)\frac{2Ba}{m\pi\Gamma_m^2}\sin\left(\frac{m\pi}{a}x\right) \cdot\sin\left(\frac{m\pi}{a}x_S\right)\sin\left(\frac{m\pi}{a}\Delta x\right) \cdot\left(e^{\Gamma_m\Delta z}-e^{-\Gamma_m\Delta z}\right)e^{-\Gamma_m|z-z_S|} \quad \text{(A2)}$$

where

$$B=\frac{120\pi c\mu k^2}{a}.$$

3) Self-contribution of conductor line cell:

$$\Delta E_y(\tilde{r}) = \sum_{m=1}^{\infty} I_S(\tilde{r}_S)\sin\left(\frac{m\pi}{a}x_S\right)\frac{1}{\Gamma_m^2\cos^2\theta+\left(\frac{m\pi}{a}\right)^2\sin^2\theta} \cdot\left\{-\Gamma_m\cos\theta\cdot\left[\sin\left(\frac{m\pi}{a}\overline{x_S-\Delta\sin\theta}\right)+\sin\left(\frac{m\pi}{a}\overline{x_S+\Delta\sin\theta}\right)\right]e^{-\Gamma_m\Delta\cos\theta} +\frac{m\pi}{a}\sin\theta\left[\cos\left(\frac{m\pi}{a}\overline{x_S-\Delta\sin\theta}\right)-\cos\left(\frac{m\pi}{a}\overline{x_S+\Delta\sin\theta}\right)\right] \cdot e^{-\Gamma_m\Delta\cos\theta}+2\Gamma_m\cos\theta\sin\left(\frac{m\pi}{a}x_S\right)\right\}. \quad \text{(A3)}$$

4) The contribution of conductor line cell to other field point:

$$\Delta E_y(\tilde{r}) = \sum_{m=1}^{\infty}\frac{I_S(\tilde{r}_S)\sin\left(\frac{m\pi}{a}x\right)e^{-\Gamma_m|z-z_S|}}{\left(\frac{m\pi}{a}\right)^2\sin^2\theta+\Gamma_m^2\cos^2\theta} \cdot\left\{\left[\frac{m\pi}{a}\sin\theta\cos\left(\frac{m\pi}{a}\overline{x_S-\Delta\sin\theta}\right)-\Gamma_m\cos\theta\sin\left(\frac{m\pi}{a}\overline{x_S-\Delta\sin\theta}\right)\right]e^{-\Gamma_m\Delta\cos\theta} -\left[\frac{m\pi}{a}\sin\theta\cos\left(\frac{m\pi}{a}\overline{x_S+\Delta\sin\theta}\right)-\Gamma_m\cos\theta\sin\left(\frac{m\pi}{a}\overline{x_S+\Delta\sin\theta}\right)\right]e^{\Gamma_m\Delta\cos\theta}\right\}. \quad \text{(A4)}$$

REFERENCES

[1] J. Schwinger, and D. Saxon, *Discontinuities in Wave Guides* (Documents on Modern Physics). New York: Gordon and Greach, 1968.

[2] N. Marcuvitz, *Waveguide Handbook*.

[3] Y.-C. Shih, "Design of waveguide E-plane filters with all-metal inserts," *IEEE Trans. Microwave Theory Tech.*, vol. MTT-32, pp. 695–704, July 1984.

[4] Y. Leviatan, P. G. Li, A. T. Adams, and J. Perini, "Single-post inductive obstacle in rectangular waveguide," *IEEE Trans. Microwave Theory Tech.*, vol. MTT-31, pp. 806–812, Oct. 1983.

[5] H. Auda and R. F. Harrington, "Inductive posts and diaphragms of arbitrary shape and number in a rectangular waveguide," *IEEE Trans. Microwave Theory Tech.*, vol. MTT-32, pp. 606–613, June 1984.

[6] C. G. Hsu and H. A. Auda, "Multiple dielectric posts in a rectangular waveguide," *IEEE Trans. Microwave Theory Tech.*, vol. MTT-34, pp. 883–891, Aug. 1986.

[7] N. Sahalos and E. Vafiadis, "On the narrow-band microwave filter design using a dielectric rod," *IEEE Trans. Microwave Theory Tech.*, vol. MTT-33, pp. 1165–1171, Nov. 1985.

[8] F. Arndt, *Proc. Inst. Elec. Eng.*, vol. 133, pp. 169–174, June 1986.

[9] J. Bornemann, *Proc. Inst. Elec. Eng.*, vol. 133, pp. 103–107, Apr. 1986.

[10] R. Vahldieck and W. R. Hoefer, "Finline and metal insert filters with improved passband separation and increased stopband attenuation," *IEEE Trans. Microwave Theory Tech.*, vol. MTT-33, pp. 1333–1339, Dec. 1985.

[11] J. Uher, F. Arndt, and J. Bornemann, "Field theory design of ferrite-loaded waveguide nonreciprocal phase shifters with multisection ferrite or dielectric slab impedance transformers," *IEEE Trans. Microwave Theory Tech.*, vol. MTT-35, pp. 552–560, June 1987.

Pong Fan was born in Anhui, Republic of China, on December 22, 1963. He received the B.Sc. degree from Anhui University in 1981 and the M.Sc. degree from the University of Science and Technology of China, Hefei, Anhui, in 1988, both in radio electronics. His research interests include the analysis and design of microwave and millimeter-wave components.

Desen Fan graduated from the Department of Radio-Electronics, Qinghua University, in 1961. Since then, he has been with the Department of Electronics, University of Science and Technology of China, Hefei, Anhui, working in the fields of electromagnetics and microwave theory and techniques. His research interests include computer techniques for electromagnetics, the computer-aided design of microwave circuits, millimeter-wave devices, and applications. Recently his work has centered on super high Q factor cavities, including high-T_c superconducting cavities, and their applications.